JOC Featured Article

The Proton Complex of a Diaza-macropentacycle: Structure, Slow Formation, and Chirality Induction by Ion Pairing with the Optically Active 1,1′-Binaphthyl-2,2′-diyl Phosphate Anion

Clément Bonnot,[†] Jean-Claude Chambron,[†,*] Enrique Espinosa,[†,‡] Klaus Bernauer,[§] Ulrich Scholten,[§,⊥] and Roland Graff[#]

Institut de Chimie Moléculaire de l'Université de Bourgogne (ICMUB, UMR CNRS no. 5260), 9 Avenue Alain Savary, BP 47870, F-21078 Dijon, France, Institut de Chimie, Université de Neuchâtel, Av. Bellevaux 51, CP 2, CH-2007 Neuchâtel, Switzerland, and Institut de Chimie (UMR CNRS no. 7177), Université Louis Pasteur, 1 rue Blaise Pascal, 67000 Strasbourg, France

jean-claude.chambron@u-bourgogne.fr

Received July 3, 2008

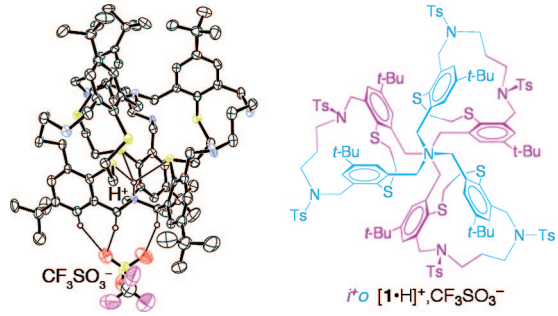

The protonation of a sterically crowded [N_2S_6] macropentacycle (**1**) with 1 equiv of CF_3SO_3H in $CDCl_3$ is slow and gives the singly (oo^+ [**1**•H]$^+$) and doubly (o^+o^+ [**1**•2H]$^{2+}$) protonated forms as kinetic products, the i^+o form of [**1**•H]$^+$ being the thermodynamic product. i^+o [**1**•H]$^+$ is C_3 helically chiral in the solid state and in solution. The barrier to racemization ($\Delta G^{\ddagger}$) of the [**1**•H]$^+$ propeller is >71 kJ mol^{-1}. The ammonium proton is encapsulated in the tetrahedral coordination sphere provided by the *endo* (*i*) nitrogen bridgehead atom and the three proximal thioether sulfurs, which makes [**1**•H]$^+$ a proton complex. Use of the optically active acid (*R*)-(−)- or (*S*)-(+)-1,1′-binaphthyl-2,2′-diyl hydrogen phosphate (BNPH) in chloroform allowed us to induce a significant diastereomeric excess (24% de), which produced a detectable ICD. The de was decreased in acetone-d_6 (10%), suggesting that the sense of chirality of [**1**•H]$^+$ is controlled by ion-pair interactions. Detailed NMR studies allowed us to locate the chiral anion on the *endo* side of [**1**•H]$^+$, in the cavity lined by *endo* *t*-Bu groups, and to establish that the rate of anion exchange in [**1**•H][(*S*,*R*)-(±)-BNP] was higher than the rate of propeller inversion of [**1**•H]$^+$.

Introduction

The protonation of diaza-macrobicycles[1−3] and related systems, such as cryptands[4−8] (Figure 1) has been studied in detail. These hollow molecules may exist under three different isomeric forms (the so-called homeomorphic isomers),[1,9] depending on the inside (*in*) or outside (*out*) orientation of the lone pairs of the bridgehead nitrogen atoms with respect to the cavity: *in, in* (*ii*); *in*, *out* (the degenerate *io* and *oi);* and *out*, *out* (*oo*). For example, symmetrical 1,(*k*+2)-diazabicyclo[*k.l.m*]alkanes ([*k.l.m*]-**2**, $k = l = m$) exist in the *ii* form when $k \geq 4$,[2c] as well as cryptand [1.1.1]-**3**.[5] The study of unsymmetrical [*k*.3.1]-**2** (a family of tetrahydropyrimidines) has permitted us to identify a

[†] Université de Bourgogne.
[§] Université de Neuchâtel.
[#] Université Louis Pasteur.
[‡] Current address: LCM3B (UMR CNRS no. 7036), Nancy Université, 1 Boulevard des Aiguillettes, 54506 Vandœuvre-lès-Nancy, France.
[⊥] Current address: Département des technologies industrielles, Ecole d'ingénieurs et d'architectes, Pérolles 80, CP 32, CH-1705 Fribourg, Switzerland.

10.1021/jo801438d CCC: $40.75 © 2008 American Chemical Society
Published on Web 09/24/2008

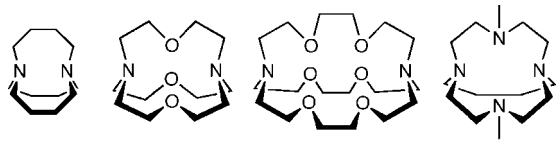

FIGURE 1. Examples of macrobicycles with nitrogen bridgeheads.

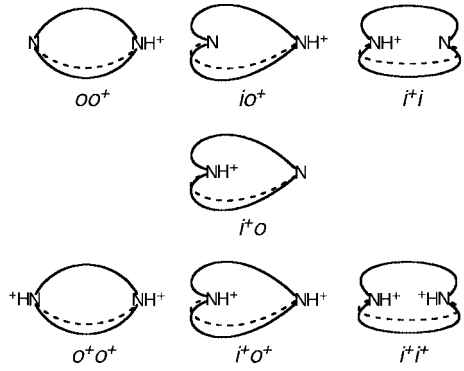

FIGURE 2. Nomenclature of the different protonated forms of diaza-macrobicycles.

transition between the symmetrical *oo* ($k = 5$) and unsymmetrical *io* ($k = 7$) forms.[10]

Double protonation of diaza-macrobicycles translates directly the three forms identified above into i^+i^+, i^+o^+, and o^+o^+, respectively, while single protonation can produce up to four different forms: i^+i, i^+o, io^+, and oo^+ (Figure 2). Interconversion between these forms involves various acid/base equilibria and the nitrogen inversion process.[1b]

Early studies of [*k.l.m*]-**2** had shown that the o^+o^+ diprotonated species that was formed in 50% aqueous CF_3CO_2D converted to the i^+i^+ isomer slowly (3 days).[1a] Similar results were found by recent investigations, which used a controlled excess (~3 equiv) of CF_3CO_2D in anhydrous conditions (CD_2Cl_2) at 0 °C. For example, in the case of [6.6.4]-**2**, a 50:50 mixture of i^+o^+ and o^+o^+ diprotonated species formed immediately, which, upon warming the reaction mixture to room temperature (25 °C), gradually (~1 d) converted to the i^+i^+ isomer.[3b] Various doubly protonated cryptands[6c,7,8] and prismand[3a] crystallized in the i^+i^+ form as shown by X-ray diffraction. Single protonation was also studied. Reaction of 1 equiv of CF_3CO_2H in $CDCl_3$ with [*k.l.m*]-**2** produced the i^+i form of the larger ring systems (e.g., [5.4.2]-**2**), also at slow rates (0.5 h at 35 °C).[2b] Whereas inside protonation was not observed for the smallest ring systems (e.g., [5.3.2]-**2**), intermediate size derivatives, such as [4.4.4]-**2**, converted slowly to the i^+i form in oxidizing conditions, where a redox-promoted rearrangement operates.[2a] Single protonation of cryptand [1.1.1]-**3** to form the io^+ species is fast, but conversion of the latter to the i^+i isomer has a rate constant of 2.3×10^{-4} s^{-1} only, at pD 3.2.[5c] The N*H*$^+$ resonance of these singly protonated small diaza-macrobicycles appears at lower field than usually observed because of NH$^+$···N hydrogen bonding with the opposite bridgehead nitrogen.[2b,4d] The concealed proton does not exchange with solvent protons and can be hardly removed in some cases, which ranks the corresponding free base macrobicycles among the strongest proton sponges.[2a,4d,5c] All these results were interpreted in terms of kinetic and thermodynamic control of the protonation reactions: initial *exo* protonation is under kinetic control, whereas delayed *endo* protonation is under thermodynamic control.[3b]

Protonated diaza-macrobicycles can, in principle, have D_3- or C_3-symmetric conformations, as other macrobicyclic propellers.[11−13] However, this helical chirality is usually not realized in solution, even on the NMR time scale, but has been observed in the crystal. For example, diprotonated cryptate ([2.2.2]-**3**·2H)Cl_2,[7a] which crystallizes in the symmetrical i^+i^+ form with two intraionic trifurcated N$^+$-H···O hydrogen bonds, is D_3 helically chiral as a consequence of the twisting of the bridging chains.

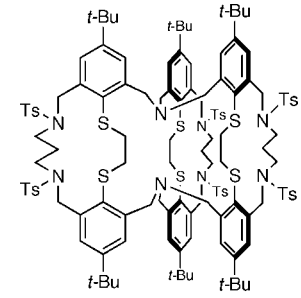

1

Macropentacycle **1**, a sterically crowded molecular cage related to cryptands, shows remarkable solution dynamics and protonation properties.[14] Its room-temperature ^{1}H NMR spectrum displays broad features that are indicative of relatively slow motions on the NMR time scale. At high temperature (380 K),

(1) (a) Simmons, H. E.; Park, C. H. *J. Am. Chem. Soc.* **1968**, *90*, 2427–2429. (b) Park, C. H.; Simmons, H. E. *J. Am. Chem. Soc.* **1968**, *90*, 2429–2431. (c) Park, C. H.; Simmons, H. E. *J. Am. Chem. Soc.* **1968**, *90*, 2431–2432. (d) Simmons, A. E.; Park, C. H.; Uyeda, R. T.; Habibi, M. F. *Trans. N. Y. Acad. Sci. Ser. II* **1970**, *32*, 521–534.

(2) (a) Alder, R. W.; Casson, A.; Sessions, R. B. *J. Am. Chem. Soc.* **1979**, *101*, 3652–3653. (b) Alder, R. W.; Moss, R. E.; Sessions, R. B. *J. Chem. Soc., Chem. Commun.* **1983**, 997–998. (c) Alder, R. W.; Orpen, A. G.; Sessions, R. B. *J. Chem. Soc., Chem. Commun.* **1983**, 999–1000.

(3) (a) Kunze, A.; Gleiter, R.; Rominger, F. *Chem. Commun.* **1999**, 171–172. (b) Pool, B.; Balalaie, S.; Kunze, A.; Schilling, G.; Bischof, P.; Gleiter, R. *Eur. J. Org. Chem.* **2004**, *281*, 2812–2817. (c) Kunze, A.; Balalaie, S.; Gleiter, R.; Rominger, F. *Eur. J. Org. Chem.* **2006**, *294*, 2942–2955.

(4) (a) Ciampolini, M.; Micheloni, M.; Vizza, F.; Zanobini, F.; Chimichi, S.; Dapporto, P. *J. Chem. Soc., Dalton Trans.* **1986**, 505–510. (b) Bianchi, A.; Garcia-España, E.; Micheloni, M.; Nardi, N.; Vizza, F. *Inorg. Chem.* **1986**, *25*, 4379–4381. (c) Bianchi, A.; Ciampolini, M.; Micheloni, M.; Nardi, N.; Valtancoli, B.; Mangani, S.; Garcia-España, E.; Ramirez, J. A. *J. Chem. Soc., Perkin Trans. 2* **1989**, 1131–1137. (d) Bencini, A.; Bianchi, A.; Bazzicalupi, C.; Ciampolini, M.; Dapporto, P.; Fusi, V.; Micheloni, M.; Nardi, N.; Paoli, P.; Valtancoli, B. *J. Chem. Soc., Perkin Trans. 2* **1993**, 115–120.

(5) (a) Cheney, J.; Lehn, J.-M. *J. Chem. Soc., Chem. Commun.* **1972**, 487–489. (b) Cheney, J.; Kintzinger, J.-P.; Lehn, J.-M. *Nouv. J. Chim.* **1978**, *2*, 411–418. (c) Smith, P. B.; Dye, J. L.; Cheney, J.; Lehn, J.-M. *J. Am. Chem. Soc.* **1981**, *103*, 6044–6048.

(6) (a) Pitzer, R. *J. Am. Chem. Soc.* **1978**, *100*, 4239–4241. (b) Cox, B. G.; Murray-Rust, J.; Murray-Rust, P.; van Truong, N.; Schneider, H. *J. Chem. Soc., Chem. Commun.* **1982**, 377–379. (c) Brügge, H.-J.; Carboo, D.; von Deuten, K.; Knöchel, A.; Kopf, J.; Dreissig, W. *J. Am. Chem. Soc.* **1986**, *108*, 107–112.

(7) (a) MacGillivray, L. R.; Atwood, J. L. *J. Org. Chem.* **1995**, *60*, 4972–4973. (b) MacGillivray, L. R.; Atwood, J. L. *Chem. Commun.* **1996**, 735–736. (c) MacGillivray, L. R.; Atwood, J. L. *Angew. Chem., Int. Ed. Engl.* **1996**, 1828–1830.

(8) Morehouse, P.; Hossain, M. A.; Llinares, J. M.; Powell, D.; Bowman-James, K. *Inorg. Chem.* **2003**, *42*, 8131–8133.

(9) Alder, R. W.; East, S. P. *Chem. Rev.* **1996**, *96*, 2097–2111.

(10) Alder, R. W.; Heilbronner, E.; Honegger, E.; McEwen, A. B.; Moss, R. E.; Olefirowicz, E.; Petillo, P. A.; Sessions, R. B.; Weisman, G. R.; White, J. M.; Yang, Z.-Z. *J. Am. Chem. Soc.* **1993**, *115*, 6580–6591.

(11) (a) Nakazaki, M.; Yamamoto, K.; Toya, T. *J. Org. Chem.* **1981**, *46*, 1611–1615. (b) O'Krongly, D.; Denmeade, S. R.; Chiang, M. Y.; Breslow, R. *J. Am. Chem. Soc.* **1985**, *107*, 5544–5545. (c) Wallon, A.; Werner, U.; Müller, W. M.; Nieger, M.; Vögtle, F. *Chem. Ber.* **1990**, *123*, 859–867. (d) L'Esperance, R. P.; West, A. P., Jr.; Van Engen, D.; Pascal, R. A., Jr. *J. Am. Chem. Soc.* **1991**, *113*, 2672–2676.

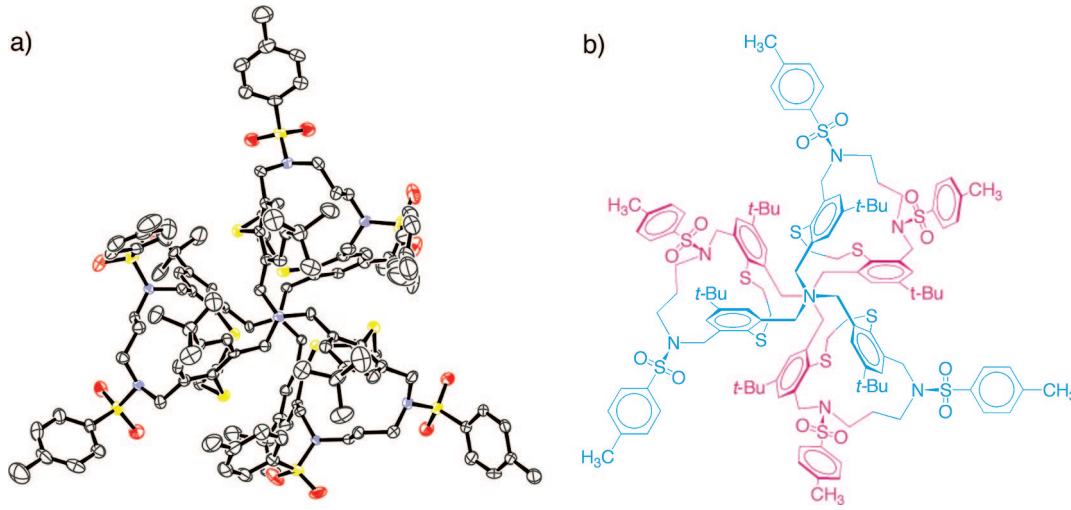

FIGURE 3. Top views from the *exo* bridgehead nitrogen of the solid-state structure of singly protonated macropentacycle [**1**·H](CF_3SO_3). (a) ORTEP view of the X-ray crystal structure. Counterion, hydrogen atoms, and solvent molecules have been omitted for clarity. Thermal ellipsoids are drawn at 50% probability. (b) Schematic drawing. The *exo (o)* and *endo (i)* sides of the molecule are colored in cyan and magenta, respectively. The *endo* bridgehead nitrogen and the encapsulated proton are hidden by the *exo* bridgehead nitrogen because they lie on the C_3 symmetry axis (see Figure 4a).

the average maximum D_{3h} symmetry is reached, but at low temperature (200 K) as well as in the solid state, the molecule displays the *io* conformation and is C_1 asymmetric.[14b] Likewise, the monoprotonated species [**1**·H]$^+$ has the i^+o conformation, the proton being bound to the *endo* (*i*) nitrogen and the three proximal sulfurs, but is a C_3-symmetric propeller in the solid state (single-crystal X-ray diffraction) and in solution at room temperature (^{1}H NMR). A significant, solvent dependent, helical sense bias could be induced using 1 equiv of (*R*)-(−)-1,1′-binaphthyl-2,2′-diyl hydrogen phosphate (BNPH): from a maximum value of 24% de in $CDCl_3$ it was decreased to 10% de in more polar acetone-d_6,[14a] indicating that the diastereoselectivity was controlled by ion pair effects, as a particular case of the Pfeiffer effect[15] in coordination chemistry, recently developed by Lacour and co-workers.[16]

This study reports in detail on the properties of the proton complex [**1**·H]$^+$ of macropentacycle **1**: correlation between the structures in the solid state and in solution, slow kinetics of formation, induction of the sense of chirality by optically active 1,1′-binaphthyl-2,2′-diyl phosphate, and solution structure of the [**1**·H]$^+$/BNP$^-$ ion pair.

(12) (a) Rubin, Y.; Parker, T. C.; Khan, S. I.; Holliman, C. L.; McElvany, S. W. *J. Am. Chem. Soc.* **1996**, *118*, 5308–5309. (b) Ilioudis, C. A.; Bearpark, M. J.; Steed, J. W. *New J. Chem.* **2005**, *29*, 64–67. (c) Conejo-Garciá, A.; Campos, J.; Eder, C.; Entrena, A.; Gallo, M. A.; Espinosa, A. *J. Org. Chem.* **2005**, *70*, 5748–5751.

(13) (a) Alajarín, M.; López-Lázaro, A.; Vidal, A.; Berná, J. *Chem.—Eur. J.* **1998**, *4*, 2558–2570. (b) Alajarín, M.; López-Leonado, C.; Vidal, A.; Berná, J.; Steed, J. W. *Angew. Chem., Int. Ed.* **2002**, *41*, 1205–1207. (c) Perkins, D. F.; Lindoy, L. F.; Meehan, G. V.; Turner, P. *Chem. Commun.* **2004**, 152–153. (d) Tominaga, M.; Masu, H.; Katagiri, K.; Kato, T.; Azumaya, I. *Org. Lett.* **2005**, *7*, 3785–3787. (e) Haberhauer, G.; Oeser, T.; Rominger, F. *Chem.—Eur. J.* **2005**, *11*, 6718–6726.

(14) (a) Bonnot, C.; Chambron, J.-C.; Espinosa, E. *J. Am. Chem. Soc.* **2004**, *126*, 11412–11413. (b) Bonnot, C.; Chambron, J.-C.; Espinosa, E.; Graff, R. *J. Org. Chem.* **2008**, *73*, 868–881.

(15) (a) Pfeiffer, P.; Quehl, K. *Chem. Ber.* **1931**, 2667–2671. (b) Gyarfas, E. C.; Dwyer, F. P. *Rev. Pure Appl. Chem.* **1954**, *4*, 73–76. (c) Kirschner, S.; Ahmad, N. *J. Am. Chem. Soc.* **1968**, *90*, 1910–1911.

(16) (a) Lacour, J.; Jodry, J. J.; Ginglinger, C.; Torche-Haldimann, S. *Angew. Chem., Int. Ed.* **1998**, *37*, 2379–2380. (b) Lacour, J.; Jodry, J. J.; Monchaud, D. *Chem. Commun.* **2001**, 2302–2303. (c) Vial, L.; Lacour, J. *Org. Lett.* **2002**, *4*, 3939–3942. (d) Hebbe-Viton, V.; Desvergnes, V.; Jodry, J. J.; Dietrich-Buchecker, C.; Sauvage, J.-P.; Lacour, J. *Dalton Trans.* **2006**, 2058–2065. (e) Habermehl, N. C.; Angus, P. M.; Kilah, N. L.; Norén, L.; Rae, A. D.; Willis, A. C.; Wild, S. B. *Inorg. Chem.* **2006**, *45*, 1445–1462.

Results and Discussion

The i^+o form of [**1**·H]$^+$ was discovered by serendipity: careful examination of the solid material that had deposited from a solution of macropentacycle **1** in dichloromethane/heptane 20:80 v/v after a week showed that it consisted of an amorphous precipitate, which was flecked with well-shaped crystals. The solids were separated mechanically and analyzed. Thin-layer chromatography (SiO_2, dichloromethane/methanol 98:2 v/v) indicated that the crystallized product (R_f = 0.19) was much more polar than the precipitated amorphous solid (R_f = 0.76), which was analyzed as the free base macropentacycle **1**. Evidence that the crystalline material resulted from single protonation of **1** by residual HCl in the solvent was supported by comparison of its ^{1}H NMR spectrum with those obtained by mixing equimolar amounts of **1** and either trifluoromethanesulfonic (CF_3SO_3H) or trifluoroacetic (CF_3CO_2H) acid and by the single-crystal X-ray diffraction analyses of [**1**·H](CF_3SO_3)[14a] and [**1**·H](Cl).

X-ray Crystal Structure of Monoprotonated Macropentacycle 1. Suitable crystals were obtained by slow evaporation of acetone solutions ([**1**·H](Cl)) or slow diffusion of ethylacetate in dichloromethane ([**1**·H](CF_3SO_3)). ORTEP views are displayed for [**1**·H](CF_3SO_3) in Figures 3 and 4a. They show that [**1**·H]$^+$ is a C_3-symmetric propeller and has the unsymmetrical i^+o conformation in the solid state.[14a] The ammonium proton is located on the *endo* bridgehead nitrogen atom (N1), and its position could be refined within the [NS_3] coordination sphere. It is bound to the three proximal thioether sulfur atoms, with an average H···S distance of 2.58 Å, the shortest and the longest being, respectively, 2.46 (H···S1c) and 2.65 Å (H···S1b), both in [**1**·H](Cl) (Figure S1a and Table S1, Supporting Information). This makes [**1**·H]$^+$ a proton complex rather than a protonated tertiary amine. The lone pair of the *exo* bridgehead nitrogen atom (N4) is buried in the hydrophobic pocket lined by the *t*-Bu substituents, and hydrogen bonds with the *o*-aryl C−H's, with an average H···N distance of 2.43 Å, the shortest and the longest being respectively 2.38 (H2b···N4) and 2.48 Å (H2a···N4) for [**1**·H](CF_3SO_3) (Figure S1b and Table S1, Supporting Information). On the contrary, the *t*-Bu groups of

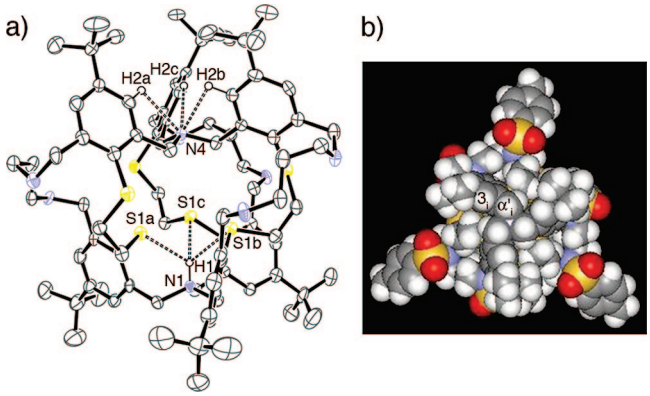

FIGURE 4. X-ray crystal structure of [**1**·H](CF_3SO_3). (a) ORTEP side view. Ts groups, hydrogen atoms other than those highlighted, and counterions are omitted for clarity. Thermal ellipsoids are drawn at 50% probability level. (b) CPK view from the *endo* side of the molecule.

the *endo* side point away from each other, leaving an open cavity the bottom of which is lined with three axial (N1)C*H* and aromatic protons hereafter labeled α'_i and 3_i, respectively (Figure 4b). The counterions are located on this side of $[\mathbf{1}\cdot H]^+$ at a distance from the N1 atom of 4.46 Å for Cl^-, and for the two closest oxygen atoms of $CF_3SO_3^-$, which are each equally disordered over two positions, 3.75 and 3.92 Å (respectively 3.88 and 3.79 Å). In addition, they lie off the (N1, N4) axis, at 2.00 and 0.80 Å, respectively (Figure S2, Supporting Information). The anions are hydrogen-bound to one of the three benzylic protons α'_i mentioned above (at 2.58 Å for Cl^-, and at 2.54 and 2.50 Å for $CF_3SO_3^-$), which, due to the positive charge on N1, display an electron acceptor character. Close contacts with aromatic proton 3_i (3.16 Å for Cl^- and 2.48 Å for $CF_3SO_3^-$) are also observed (Figure S3, Supporting Information).

The triple-helical structure is apparent from the top views of Figure 3. Helicity is expressed in the orientation of the benzylic $N(CH_2Ar)_3$ *exo* and *endo* bridgehead propellers, the tilt of the Ar spacers, and the twist of the bridging macrocyclic branches, which are mechanically linked. Remarkably, the orientation of the *exo* $N(CH_2Ar)_3$ propellers (*M* in Figure 3) is opposite to that of the *endo* ones (*P*). The triple helices of [**1**·H](Cl) and [**1**·H](CF_3SO_3) are characterized by the torsion angle θ which, for each branch of the molecule, corresponds to <C−N1−N4−C> (Figure S1b and Table S1, Supporting Information). Its average value is 57° for [**1**·H](Cl), higher than the value measured for [**1**·H](CF_3SO_3) (49°). However, in both cases, the distances between the bridgehead nitrogen atoms are close to 6.33 Å. Without the tosyl groups, a noncrystallographic C_3 molecular symmetry exhibits along the (N1, N4) direction (Figure S4 and Tables S2 and S3, Supporting Information).

In the case of [**1**·H](CF_3SO_3), all the Ts substituents are oriented along the (*endo*-N1, *exo*-N4) direction, the Ts of the *exo* side being equatorial and those of the *endo* side being axial and folded up in the grooves formed by two consecutive branches of the triple helix (Figure 3). A similar situation is observed for [**1**·H](Cl), except that one of the *endo* Ts is oriented downward, thus destroying the 3-fold symmmetry in the crystalline state (Figure S2b, Supporting Information).

In summary, the encapsulated proton that brings the three proximal thioether sulfur atoms to order completely controls the molecular structure of $[\mathbf{1}\cdot H]^+$ by mechanical (steric and strain) effects: (i) the molecule takes up a C_3 symmetric structure with a helical twist and (ii) the *endo* Ar and *exo* Ar spacers are placed in opposite directions, the former being directed away from each other while the latter are brought closer together, allowing for weak (C)H···N interactions.

Solution Structure of Monoprotonated Macropentacycle $[\mathbf{1}\cdot H]^+$. This section demonstrates that the molecular structure of $[\mathbf{1}\cdot H]^+$ in solution (^1H and ^{13}C NMR) is fully consistent with the structure established by X-ray crystallography. The room temperature ^1H NMR spectrum of [**1**·H](CF_3CO_2) in CD_2Cl_2 is shown in Figure 5 (proton labeling in Figure 6). Complete attribution was achieved using bidimensional ($^1H/^1H$ COSY and ROESY, $^{13}C/^1H$ HSQC and HMBC) experiments (Figures S5−S13, Supporting Information). COSY correlations (Figures S5 and S6, Supporting Information) allowed us, in particular, to establish a 1:1 pairwise relationship between geminal protons of each methylenic system (that is, *in* (*i*) and *out* (*o*) α/α', β/β', γ/γ', δ/δ', and ε/ε'), which was confirmed by HSQC (Figure S11, Supporting Information). Several COSY correlations between vicinal protons of these systems were also observed, namely δ/γ_i, δ/γ'_i, δ'/γ_o, δ'/γ'_i, and $\varepsilon'_i/\varepsilon_o$ for the strongest ones. A total of 18 signals (as doublet (d), apparent triplet (t) or doublet of doublets (dd), integrating each for three protons) were identified in the aliphatic region, which could be assigned to the nine triply degenerate methylene groups of the molecule (Figure 5). Therefore, all the methylenic protons form diastereotopic (H, H′) pairs, which indicates that $[\mathbf{1}\cdot H]^+$ is chiral in solution on the ^1H NMR time scale. Given the structure of the molecule, chirality arises from the C_3 symmetry. The NH^+ signal appears as a quadruplet at 9.397 ppm, which is broadened by the quadrupole moment of nitrogen and is coupled with α'_i.[17a] The latter appears clearly as a dd pair at 5.134 ppm ($^3J(\alpha_i,\alpha'_i)$ = 13.2 Hz and $^3J(\alpha'_i,H^+)$ = 10.2 Hz), while the signal of its geminate α_i atom is a doublet at 4.422 ppm ($^3J(\alpha_i,\alpha'_i)$ = 12.0 Hz and $^3J(\alpha_i,H^+)$ = 0 Hz). Noticeably, the chemical shift of α'_i is solvent-dependent (Figure S14, Supporting Information).[17b] The dihedral ϕ angles in the bond sequence H−C−N−H^+ for α_i and α'_i are, respectively, 79° and 159°,[18] which compares reasonably well with the values obtained in the solid state (72.3° and 170.7° for [**1**·H](Cl) and 67.3° and 174.8° for [**1**·H](CF_3SO_3)). Observation of the relatively sharp quadruplet signal indicates that slow exchange conditions between acid and conjugated base are met on the NMR time scale. Indeed, the ^1H NMR spectrum of a 1:1 mixture of **1** and [**1**·H](CF_3SO_3) in $CDCl_3$ is a superposition of the spectra of the separated species. However, upon addition of D_2O, the NH^+ signal disappears and the dd signal of α'_i changes to a doublet, indicating that the ammonium proton is in fast exchange with solvent protons on the NMR time scale. Identification of the (α_i/α'_i) pair offers a starting point for progressing through the $^1H/^1H$ COSY and ROESY maps, and allows to differentiate between the *exo* (*o*) and the *endo* (*i*) halves of $[\mathbf{1}\cdot H]^+$. The $^1H/^1H$ ROESY correlations (Figures S7−S10, Supporting Information) can be fully rationalized on the basis of the X-ray crystal structure discussed above. The most significant are reported in the ORTEP view of an isolated branch of the molecule (Figure 6b). Those involving the methylenic protons (e.g., α_i/ε_i, α_i/ε'_i, β'_i/γ_i, β'_i/δ', β'_i/ε_o, γ_i/ε_o, etc.) attest to the conformation of the macrocyclic subunits. As for (α_i,α'_i)/NH^+, the stereochemical relationships between vicinal methylenic protons are the same in solution and in the crystal, as shown qualitatively in Table S5 (Supporting Information). Therefore $[\mathbf{1}\cdot H]^+$ behaves as a conformationally fixed tertiary amine, where dihedral angles are well-defined,

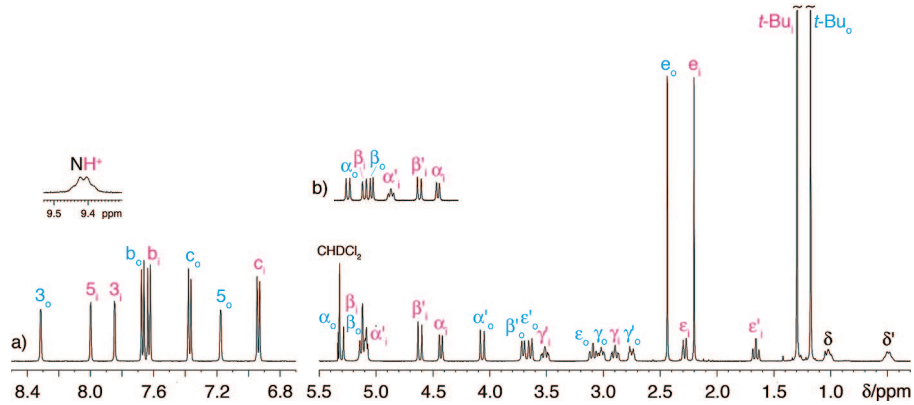

FIGURE 5. ^{1}H NMR spectrum of (a) [**1**·H](CF$_3$CO$_2$) in CD_2Cl_2 (600 MHz, 298 K); (b) [**1**·H](CF$_3$SO$_3$) in $C_2D_2Cl_4$ (500 MHz, 360 K): selected region showing separate signals for the protons α_o, α'_i, β_o, and β_i.

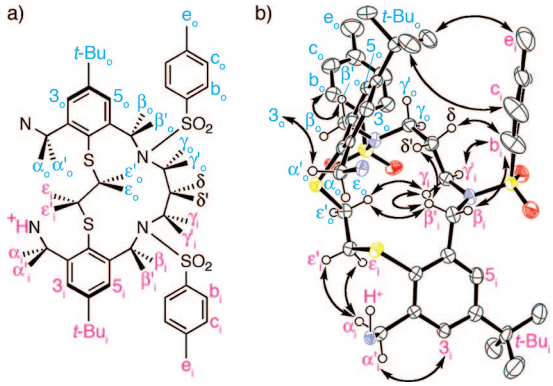

FIGURE 6. Side views of a branch of [**1**·H]$^+$. (a) Schematic drawing showing the principle of proton labeling. (b) ORTEP side view of an isolated branch of the X-ray crystal structure of [**1**·H](CF$_3$SO$_3$) with selected hydrogen atoms. Ellipsoids are drawn at 50% probability level. Double-ended arrows indicate remarquable NOE correlations.

similarly to small cycles or fused cyclic structures.[17−19] ROESY correlations involving aromatic and aliphatic protons ($3_i/\alpha_i$ and $3_i/\alpha'_i$; $5_i/\beta_i$; b_i/α'_o, b_i/β_i, b_i/γ'_i and b_i/δ; $3_o/\alpha'_o$; $5_o/\beta'_o$ and $5_o/\gamma'_o$; b_o/β'_o, and b_o/γ_o) are also informative. The four latter are consistent with the equatorial orientation of the *exo* Ts, while b_i/β_i, b_i/γ'_i, and b_i/δ agree with the axial orientation of the *endo* Ts. The folding up of these groups is also supported by the correlations *t*-Bu$_o$/c_i and *t*-Bu$_o$/e_i, which involve protons that are separated by longer topological distances (16 atoms). Conversely, the lack of any interaction between c_o (or e_o) and the rest of the molecule indicates that the *endo* Ts diverge from the core of [**1**·H]$^+$. Protons α_o, β_i, β_o and α'_i are deshielded by the adjacent *t*-BuAr subunits, while central δ' are shielded by the *exo* *t*-BuAr and the *endo* Ts. Due to the quasi-parallel orientation of the latter aromatic rings, protons c_i and e_i are shielded by comparison with c_o and e_o of the *exo* Ts groups (respectively by −0.424 and −0.231 ppm). The aromatic protons 3_o are considerably deshielded with respect to 5_o ($\Delta\delta = +1.131$ ppm) probably because of their intramolecular hydrogen bonding with the *exo* bridgehead nitrogen atom, as revealed in the X-ray crystal structure. The C_3 symmetry of i^+o [**1**·H]$^+$ is also apparent from the ^{13}C NMR spectrum, which shows the 35 expected carbon signals (Figures S15−S17, Supporting Information).

In summary, NMR studies show that the monoprotonated macropentacycle [**1**·H]$^+$ has a C_3 symmetric triple helical i^+o conformation in solution at room temperature and on the NMR time scale. Increasing the temperature up to 380 K ($C_2D_2Cl_4$; Figure S18, Supporting Information) slightly decreases the separation between diastereotopic protons, with few exceptions (α_i,α'_i and γ_i,γ'_i). Coalescence phenomena that would exchange mirror-image helical conformations on the one hand, the i^+o and oi^+ forms on the other hand, must occur at higher temperature on the ^{1}H NMR time scale. The minimal $\Delta G_c^{\ddagger}$ value for these processes can be estimated to ∼ 71 kJ mol^{-1} (17.0 kcal mol^{-1}), based on the diastereotopic pair of protons (α_o,α'_o).[20] Decreasing the temperature down to 200 K (CD_2Cl_2; Figure S19, Supporting Information) broadens most of the signals, with the exception of those of the *exo* Ts groups, and leads to a spectrum that is reminiscent of the spectrum obtained for neutral macropentacycle **1** in the same conditions. This is not surprising, as the latter was shown to adopt a C_1 pseudohelical *io* conformation at low temperature, that shares several common features with i^+o [**1**·H]$^+$.[14b]

Slow Kinetics of Formation of i^+o [1·H]$^+$. Whereas protonation of macropentacycle **1** by trifluoracetic acid (pK_a = 12.7 in CH_3CN)[21a] is immediate in $CDCl_3$, reaction with stronger trifluoromethanesulfonic acid ($pK_a = 2.60$)[21b] is slow enough to allow the reaction to be monitored by ^{1}H NMR. The sequence of high field (*t*-Bu) and low field (N*H*$^+$) regions of the spectra obtained after addition of ∼1 equiv of CF_3SO_3H to a dry $CDCl_3$ solution of **1** is displayed in Figure 7 (Other regions of the spectra are shown in Figures S20−S23, Supporting Information). On the basis of the analysis of the *t*-Bu and N*H*$^+$ signals (number and relative integrations; Figures S24 and S25, Supporting Information), four different species can be identified ∼1 h after addition of acid: starting neutral **1** (green dot), singly protonated (red dot) i^+o [**1**·H]$^+$ (δ(N*H*$^+$) = 9.35 ppm), another singly protonated (blue dot) [**1**·H]$^+$ species (δ(N*H*$^+$) = 10.21

(17) (a) Booth, H.; Little, J. H. *J. Chem. Soc., Perkin Trans. 2* **1973**, 1846–1853. (b) Also sensitive to the medium (solvent, counteranion) are the chemical shifts of protons 3_i and 5_i.

(18) The following Karplus relationship was used: $9.8\cos^2\phi - 1.8\cos\phi - J = 0$: Fraser, R. F.; Renaud, R. N.; Saunders, J. K.; Wigfield, Y. Y. *Can. J. Chem.* **1973**, *51*, 2433–2437.

(19) (a) Lambert, J. B.; Keske, R. G.; Weary, D. K. *J. Am. Chem. Soc.* **1967**, *89*, 5921–5924. (b) Riddell, F. G.; Lehn, J.-M. *J. Chem. Soc. B* **1968**, 1224–1228. (c) Lowry, B. R.; Huitric, A. C. *J. Org. Chem.* **1972**, *37*, 1316–1320.

(20) The relationship $\Delta G^{\ddagger} = RT_c(22.96 + \ln(T_c/(\Delta\nu^2 + 6J^2)^{1/2})$ was used to estimate the activation energy ($\Delta G^{\ddagger}$/kJmol^{-1}) from the coalescence temperature (T_c/K), the frequency separation of the peaks ($\Delta\nu$/Hz), and the coupling constant (J/Hz) between the nuclei (ref 16c). The corresponding k_c value is $(\pi/2^{1/2})(\Delta\nu^2 + 6J^2)^{1/2}$. For the ($\alpha_o$,$\alpha'_o$) pair, $\Delta\nu$ = 600 Hz and ^2J = 16.7 Hz in $C_2D_2Cl_4$ at the low-temperature limit (300 K).

(21) (a) Hayakawa, Y.; Iwase, T.; Nurminen, E. J.; Tsukamoto, M.; Kataoka, M. *Tetrahedron* **2005**, *61*, 2203–2209. (b) Fujinaga, T.; Sakamoto, I. *J. Electroanal. Chem. Interfac. Chem.* **1977**, *85*, 185–201.

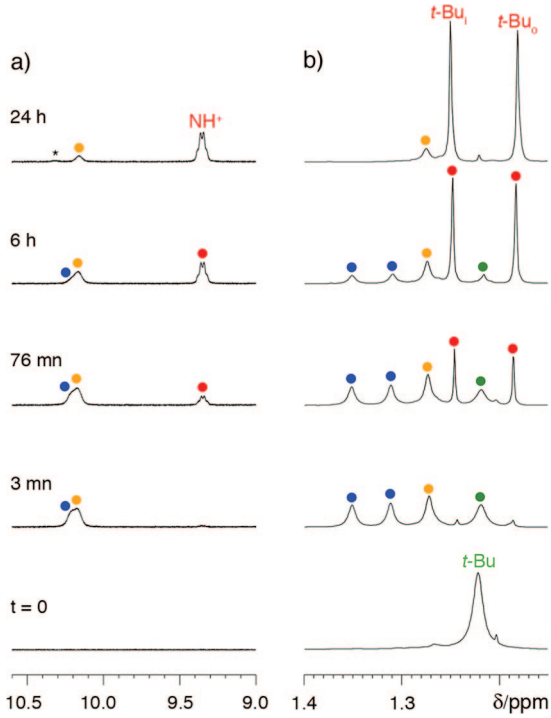

FIGURE 7. Time evolution of the ^{1}H NMR spectrum obtained after addition of CF_3SO_3H (~1 equiv) to a solution of **1** in $CDCl_3$ at 300 K. a) NH^+ and b) *t*-Bu region of the spectra. Color codes: (green dot) neutral form; (blue dot) oo^+; (red dot) i^+o; (yellow dot) o^+o^+. $t = 0$ refers to immediately before the addition of the acid.

ppm), and a *symmetrical* doubly protonated (yellow dot) $[\mathbf{1}\cdot 2H]^{2+}$ species ($\delta(NH^+) = 10.16$ ppm). The latter are tentatively assigned to the oo^+ (or io^+), and o^+o^+ forms, respectively, as *exo* NH^+ usually resonate downfield by comparison with *endo* NH^+.[1a,22] While i^+o $[\mathbf{1}\cdot H]^+$ is hardly detectable "immediately" (3 min) after addition of the acid, its concentration gradually increases at the expense of the other species. Time evolution of the distribution of the four identified species is reported in Figure 8. The "initial" (3 min) ratio between the neutral **1** (green dot), *exo* $[\mathbf{1}\cdot H]^+$ (blue dot), symmetric *exo*/*exo* $[\mathbf{1}\cdot 2H]^{2+}$ (yellow dot), and *endo* $[\mathbf{1}\cdot H]^+$ (red dot) forms is 24:39:29.5:7.5. At room temperature, the neutral macropentacycle may exist under exchanging *ii*, *io* (*oi*), and *oo* forms. Assuming that the most reactive toward protonation is the *oo* form,[1a,3b] single protonation of macropentacycle **1** would afford a 25:50:25 statistical distribution for *oo*, oo^+ (o^+o), and o^+o^+. Since the $t = 3$ min distribution does not include the *endo* $[\mathbf{1}\cdot H]^+$ (red dot) form, these ratios are close to the distribution obtained for neutral **1**, *exo* $[\mathbf{1}\cdot H]^+$, and symmetrical *exo* $[\mathbf{1}\cdot 2H]^{2+}$. Therefore, the latter can be safely identified as the o^+o (blue dot) and o^+o^+ (yellow dot) forms. The neutral and o^+o forms have completely disappeared after ~9 h, at the time the i^+o form has practically reached its maximum of concentration. Noticeably, after 24 h, there is a residual 12.5% amount (17% in CD_2Cl_2) of the o^+o^+ form, whereas a very weak broad NH^+ singlet (*) ($\delta(NH^+) = 10.32$ ppm) can be detected in the NMR spectrum of the reaction mixture, suggesting that o^+o^+ (yellow dot) $[\mathbf{1}\cdot 2H]^{2+}$ is also a transient (kinetic) species. Interestingly, rates are increased by a factor of ~6 when $CDCl_3$ is changed for CD_2Cl_2, which allows to point more easily other signals of the corresponding species (Figures S21 and S23, Supporting Information). In addition to the various protonated forms clearly identified in the ^{1}H NMR

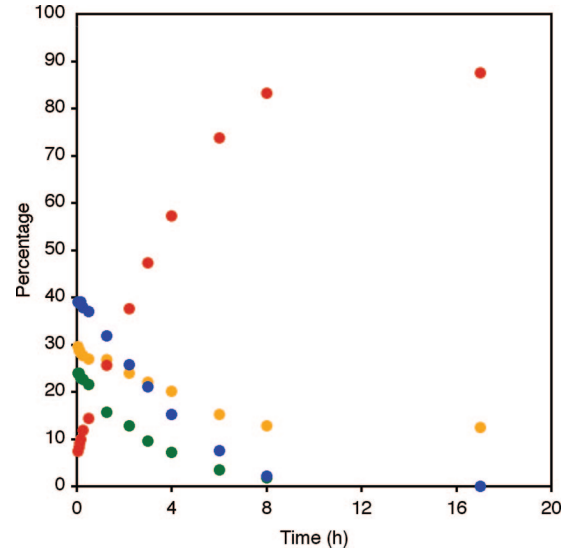

FIGURE 8. Time dependence of the relative proportions of the various protonated species identified in the series of spectra shown in Figure 7 for the protonation of **1** with CF_3SO_3H (~1 equiv). Color codes: (green dot) neutral form; (blue dot) o^+o; (red dot) i^+o; (yellow dot) o^+o^+.

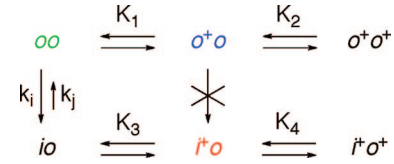

FIGURE 9. Mechanism of protonation of macropentacycle **1**.

spectra, the species i^+o^+ $[\mathbf{1}\cdot 2H]^{2+}$ should also be considered, for thermodynamic reasons. Its concentration could be very low, precluding its detection by NMR, but its formation should be as fast as that of i^+o $[\mathbf{1}\cdot H]^+$.

The analysis developed for the protonation of diaza-macrobicycles can be likewise applied to macropentacycle **1**, the *exo* protonated forms (o^+o and o^+o^+) being kinetic products, and the *endo* singly protonated form (i^+o) being the thermodynamic product of the protonation reaction.[3b] However, as inversion of protonated tertiary amines occurs after dissociation of the hydrogen ion,[1b] the direct formation of i^+o $[\mathbf{1}\cdot H]^+$ from o^+o $[\mathbf{1}\cdot H]^+$ is not possible, but rather involves *io* **1** as transient intermediate.

These kinetic measurements show two additional special features: (i) Concentration changes as a function of time show almost linear segments (for the first 8 h) and then remain suddenly constant, which means that the kinetics are close to zero order; (ii) The total amount of protonated species increases during the reaction, which means that the concentration of the free proton donor decreases concomitantly. A mechanism taking into account all these observations is proposed in Figure 9. Extrapolation of the data to zero time allows to calculate the acid dissociation constants K_1 and K_2 of o^+o^+ $[\mathbf{1}\cdot 2H]^{2+}$ as $<5.3 \times 10^{-3}$ M and $<2.6 \times 10^{-3}$ M, respectively. The result is interesting because the statistical distribution of the three species *oo*, o^+o, and o^+o^+ is obtained for $K_1 = 4K_2$. As the calculated ratio is only 2, a significant cooperative effect could be involved, the first protonation facilitating the second.[23] The trace of i^+o

(22) The *endo* NH^+ must not be deshielded by strong intramolecular hydrogen bonding.

(23) This could result from preorganization of the *exo* site of o^+o $[\mathbf{1}\cdot H]^+$ for protonation to give o^+o^+ $[\mathbf{1}\cdot 2H]^{2+}$.

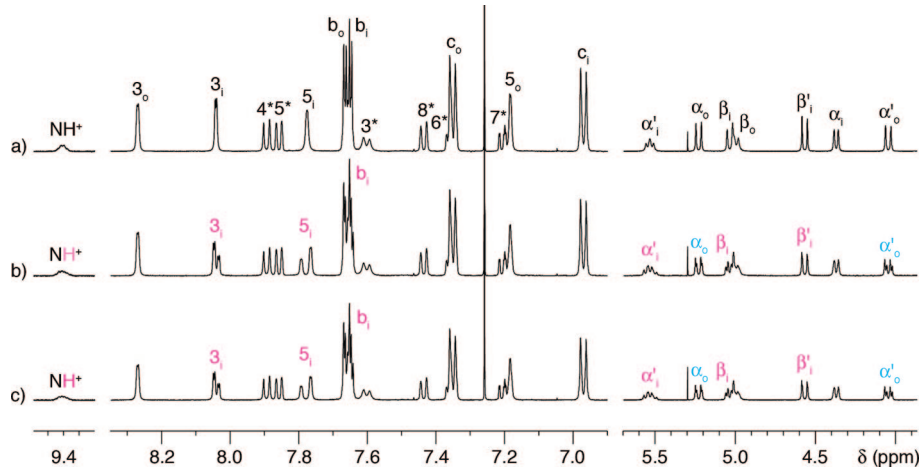

FIGURE 10. Comparison of selected regions of the ^{1}H NMR spectra (500 MHz, $CDCl_3$, 300 K) of (a) [**1**·H][(*S*,*R*)-(±)-BNP]. (b) [**1**·H][(*R*)-(−)-BNP]. (c) [**1**·H][(*S*)-(+)-BNP]. The asterisks label protons of the BNP^- anion. Labels of protons whose signals are split are colored in cyan (*exo*) and magenta (*endo*).

$[\mathbf{1}\cdot H]^+$ starting at ~5%, the unsymmetrical *io* form represents this fraction of the total amount of macropentacycle **1** before the addition of the acid. Therefore, the ratio of the rate constants k_j/k_i can be determined as ~0.05. The value of K_3 is not known, but has to be lower than K_1 and K_2; otherwise, i^+o $[\mathbf{1}\cdot H]^+$ would not be formed as the main product. As i^+o^+ $[\mathbf{1}\cdot 2H]^{2+}$ is not detected by ^{1}H NMR, $K_4 \gg K_3$. In summary, the formation of i^+o $[\mathbf{1}\cdot H]^+$ is controlled by the isomerization of the symmetric *oo* to the unsymmetrical *io* form of macropentacycle **1**.

Single protonation of **1** differs from that of strained small cage molecules, such as 1,6-diazabicyclo[4.4.4]tetradecane ([4.4.4]-**2**),[2a] cryptand [1.1.1]-**3**,[5b,c] and aza-cryptand **4**[4d] (Figure 2). The first two systems show a very slow $io^+ \rightarrow i^+i$ isomerization process, which does not correspond to a simple proton transfer in the former, but which leads to the singly protonated thermodynamic form of the latter. Another difference lies in the thermodynamic properties of these protonated bases. Whereas deprotonation is virtually impossible in all three cases, i^+o $[\mathbf{1}\cdot H]^+$ is smoothly deprotonated (4 h) using ~ 0.08 M NaOMe in 4:1 dichloromethane/MeOH solution. Its acidity constant (as triflate salt) in *acetonitrile* was estimated to lie between the values of DABCO (18.29) and cryptand [2.2.2] (18.60).[14a] Therefore, in spite of the encapsulation of the proton in the [*endo*-NS_3] cavity macropentacycle **1** behaves as a quasiordinary tertiary amine.

Induction of the Sense of Chirality. Since single protonation of **1** with Brönsted acids produced the chiral propeller i^+o $[\mathbf{1}\cdot H]^+$ (as a racemate), acids with optically active anions were next considered as proton source in order to form diastereoisomeric ion pairs and possibly induce the sense of chirality of $[\mathbf{1}\cdot H]^+$ by asymmetric transformation.[16e] 1,1′-Binaphthyl-2,2′-diyl phosphate[24] (in [(*S*,*R*)-(±)-BNP]$^-$, [(*R*)-(−)-BNP]$^-$, and [(*S*)-(+)-BNP]$^-$ forms) was selected as optically active anion because of its relatively large aromatic surfaces. The BNP^- proton adducts were generated by mixing equimolar amounts of macropentacycle **1** and 1,1′-binaphthyl-2,2′-diyl hydrogen phosphate (in optically active and racemic forms)[25] in dichloromethane/methanol 95:5 v/v and crystallized from dichloromethane/benzene.[26] The proton adducts of the optically active forms of BNPH with triethylamine were also prepared and characterized for use as references (Figures S26−S30, Supporting Information).

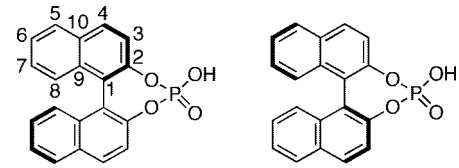

(*R*)-(−)-BNPH (*S*)-(+)-BNPH

Figure 10 compares the N*H*$^+$ and aromatic regions, and a selected part of the aliphatic region of the ^{1}H NMR spectra of the three adducts [**1**·H][(*S*,*R*)-(±)-BNP], [**1**·H][(*R*)-(−)-BNP], and [**1**·H][(*S*)-(+)-BNP] in $CDCl_3$. The spectrum of [**1**·H][(*S*,*R*)-(±)-BNP] shows the characteristic signals of $[\mathbf{1}\cdot H]^+$ and [(*S*,*R*)-(±)-BNP]$^-$. The spectra of the adducts of $[\mathbf{1}\cdot H]^+$ with the optically active anions [(*R*)-(−)-BNP]$^-$ and [(*S*)-(+)-BNP]$^-$ show two remarkable features: (i) splitting of the signals of several protons into two subsystems, and (ii) differing intensities/integrals of the two components of the split signals. The signals of the following protons show significant splittings at 600 MHz ($\Delta\delta$, ppm): the ammonium N*H*$^+$ (+0.034); in the aromatic region, 3_i (+0.015) and 5_i (−0.028); in the aliphatic region α'_i (+0.037), β_i (−0.014), β'_o (−0.010), ε'_i (+0.035), and *t*-Bu_i (−0.040). The signals of protons b_i, α_i, α_o, α'_o, β'_i, *t*-Bu_o, and e_i are also split, however by less than 0.010 ppm (Table S6, Supporting Information). Similar features can also be found in the ^{13}C NMR spectrum (Table S7, Supporting Information). These can be interpreted in terms of the presence of two diastereoisomers in each case, [(*P*)-**1**·H][(*R*)-(−)-BNP] and [(*M*)-**1**·H][(*R*)-(−)-BNP], on the one hand, [(*P*)-**1**·H][(*S*)-(+)-BNP] and [(*M*)-**1**·H][(*S*)-(+)-BNP] on the other hand, one being major (M) the other minor (m).[27] Note that the spectra

(24) (a) Jacques, J.; Fouquey, C.; Viterbo, R. *Tetrahedron Lett.* **1971**, 4617–4620. (b) Dietrich-Buchecker, C.; Rapenne, G.; Sauvage, J.-P.; De Cian, A.; Fischer, J. *Chem.—Eur. J.* **1999**, *5*, 1432–1439. (c) Warr, R. J.; Willis, A. C.; Wild, S. B. *Inorg. Chem.* **2006**, *45*, 8618–8627. (d) Eckenroad, K. W.; Thompson, L. E.; Strein, T. G.; Rovnyak, D. *Magn. Reson. Chem.* **2007**, *45*, 72–75.

(25) (*R*)-(−)-BNPH also slowly protonates macropentacycle **1** in $CDCl_3$. As CF_3SO_3H, it is a strong acid, its pK_a in H_2O being 1.0; see: Lavison, G.; Thiébaut, D. *Chirality* **2003**, *15*, 630–636. Protonation goes through a single intermediate species that is in slow exchange with the final product, [**1**·H][(*R*)-(−)-BNP].

(26) These crystals were extremely fragile and found not to be suitable for X-ray diffraction.

(27) These descriptors are purely conventional and may refer, for example, to the twist of the *endo* $N(CH_2Ar)$ propellers.

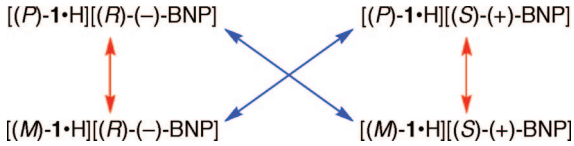

FIGURE 11. Stereoisomeric relationships between the adducts of [(*P*)-**1**•H]$^+$ and [(*M*)-**1**•H]$^+$ with [(*R*)-(−)-BNP]$^-$ and [(*S*)-(+)-BNP]$^-$. The blue and the red arrows connect enantiomers and diastereoisomers, respectively.

of the adducts of [**1**•H]$^+$ with [(*R*)-(−)-BNP]$^-$ and [(*S*)-(+)-BNP]$^-$ are identical because [(*P*)-**1**•H][(*R*)-(−)-BNP] (respectively [(*P*)-**1**•H][(*S*)-(+)-BNP]) and [(*M*)-**1**•H][(*S*)-(+)-BNP] (respectively [(*M*)-**1**•H][(*R*)-(−)-BNP]) are enantiomers (Figure 11). In other words, the major diastereoisomers (respectively minor diastereoisomers) are enantiomers of each other, whatever the optically active anion ([(*R*)-(−)-BNP]$^-$ or [(*S*)-(+)-BNP]$^-$) used. The ratio between the major and the minor diastereoisomers can be calculated from the integral ratio between the two components 5_i^M and 5_i^m of the split signal of proton 5_i, and is 62: 38, which corresponds to a diastereomeric excess (de) of 24% in $CDCl_3$ (Figure S31, Supporting Information).

The *de* slightly increased at low temperature (Figure S32, Supporting Information). For example, it was 34% at 230 K (protons 3_i^M and 3_i^m).

In light of the previous analysis, the fact that the ^{1}H NMR spectrum of [**1**•H][(*S*,*R*)-(±)-BNP] does not show the same features as those of [**1**•H][(*R*)-(−)-BNP] and [**1**•H][(*S*)-(+)-BNP] is surprising, as the four species of Figure 11 should also be present in the $CDCl_3$ solutions of [**1**•H][(*S*,*R*)-(±)-BNP]. The chemical shifts of the signals of the protons that are split in the spectra of [**1**•H][(*R*)-(−)-BNP] and [**1**•H][(*S*)-(+)-BNP] having intermediate values in the spectrum of [**1**•H][(*S*,*R*)-(±)-BNP]; this apparent contradiction can be cleared up if the ^{1}H NMR spectrum of Figure 10(a) represents the average spectrum of these four species obtained by exchange of the anions [(*R*)-(−)-BNP]$^-$ and [(*S*)-(+)-BNP]$^-$, the cation [**1**•H]$^+$ being configurationnally stable at the time scale of the experiment. In other words, the rate of anion exchange k_{ex} in [**1**•H][(*S*,*R*)-(±)-BNP] is higher than the rate of propeller inversion of [**1**•H]$^+$. A higher limit for the latter process can be calculated using the VT data obtained for [**1**•H](CF_3SO_3) in $C_2D_2Cl_4$. This allows us to set the lower limit of k_{ex} to 1345 s^{-1}.[20]

^{1}H and ^{13}C spectra in three different solvents ($CDCl_3$, CD_2Cl_2, and acetone-d_6) were fully assigned using a combination of ^{1}H/^{1}H COSY and ROESY, ^{13}C/^{1}H HSQC, and HMBC NMR experiments (Figures S33−S37 and Tables S6−S11, Supporting Information). They could be broken down into two sets of subspectra, corresponding to the major (M) and minor (m) diastereoisomers, respectively. This is illustrated in Figure 12, which shows a detail (*t*-Bu vs aromatic regions) of the ^{1}H/^{1}H ROESY NMR spectrum of [**1**•H][(*R*)-(−)-BNP] in $CDCl_3$. Complete analysis of these spectra shows that the structural features of [**1**•H]$^+$ reported above are retained upon exchanging achiral $CF_3CO_2^-$ for chiral BNP$^-$.

The influence of the nature of the solvent on the de and splittings of proton signals was next investigated. Changing $CDCl_3$ for more polar acetone-d_6 depressed the de to 10%,[14a] whereas the value obtained in CD_2Cl_2 (de = 16%) was intermediate (Figure S31, Supporting Information). These de values were left unchanged after heating to 50 °C ($CDCl_3$ and acetone-d_6) and cooling to room temperature, which suggests that the induced diastereoselectivity is under thermodynamic

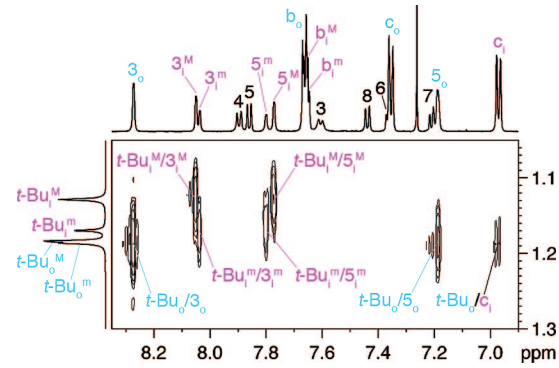

FIGURE 12. Detail of the ^{1}H/^{1}H ROESY NMR spectrum of [**1**•H][(*R*)-(−)-BNP] (600 MHz, $CDCl_3$, 298 K; mixing time: 300 ms).

control. The number of proton signals undergoing $|\Delta\delta| \geq 0.020$ ppm over the total number of split signals decreases in the order $CDCl_3$ (5/16) > CD_2Cl_2 (4/14) > acetone-d_6 (3/13). In addition, the strongest splitting (+0.037 ppm for α'_i) is observed in $CDCl_3$. The protons with split signals are highlighted in the drawings of Figure S38 (Supporting Information). In the case of the ^{13}C NMR spectra, the carbon atoms that show the strongest splittings (threshold $|\Delta\delta| \geq 0.10$ ppm) are 1_i (−0.10), 5_i (−0.12), and ε_i (+0.17) in $CDCl_3$. Comparison with the data reported above shows that the splittings observed by ^{13}C NMR do not necessarily match those observed by ^{1}H NMR. The sequence of ^{13}C NMR splittings is $CDCl_3$ (3/11) > acetone-d_6 (1/9) > CD_2Cl_2 (0/9).

Since the de and number of split proton signals decrease as the solvent polarity increases, it is likely that ion pairing of the optically active BNP$^-$ anion with [**1**•H]$^+$ is responsible for the induction of the sense of chirality of the latter by the former. The ion pair was characterized by detailed ^{1}H and ^{13}C NMR studies in the three solvents mentioned above (Tables S6−S11, Supporting Information). For example, Figure 13 compares selected regions of the ^{1}H NMR spectra of [**1**•H](CF_3CO_2) and [**1**•H][(*R*)-(−)-BNP] in acetone-d_6. Exchanging $CF_3CO_2^-$ for BNP$^-$ induces significant shifts ($\Delta\delta$, ppm) for the signals of several protons, that is: α'_i (+0.267), 3_i^m (+0.139), 3_i^M (+0.115), α_i^M (−0.111), N*H*$^+$ (−0.076), α_i^m (−0.074), *t*-Bu_i^M (−0.065), 5_i^M (−0.060), *t*-Bu_i^m (−0.059), ε_i^M (−0.055), ε_i^m (−0.048), and 5_i^M (−0.046), etc. Protons belonging to the *exo* (*o*) side of [**1**•H]$^+$ are practically unaffected, whereas protons belonging to the *endo* (*i*) side are shifted to various extents and directions: signals of protons α'_i and 3_i are shifted downfield, while practically all the other *endo* proton signals are shifted upfield, particulary those of N*H*$^+$, α_i, ε_i, 5_i, and *t*-Bu_i. These observations hold true in the case of CD_2Cl_2 and $CDCl_3$, as highlighted by the graphical representation of Figure 14. In the ^{13}C NMR spectra, the carbon atoms that show the strongest shifts whatever the solvent are 3_i-C (downfield), 5_i-C, and 6_i-C (upfield). α_i-C also shows large upfield shifts in CD_2Cl_2 and acetone-d_6 only (Tables S9 and S11, Supporting Information). All these shifts can be interpreted in terms of the magnetic anisotropy of the aromatic BNP$^-$ anion and suggest that this species is located on the endo *side* of [**1**•H]$^+$, with a negatively charged oxygen interacting with protons α'_i and 3_i, as Cl$^-$ in [**1**•H](Cl). This positions the edge of one of the naphthyl rings over a *t*-Bu_iAr group, while the other covers another *t*-Bu_i substituent, because of the twist between the two naphthyl rings. In this way, protons 3_i and α'_i, which line the bottom of the *endo* cavity (Figure 4b), are placed in the deshielding region of the first binaphthyl aromatic ring, whereas the *t*-Bu_i protons, which form the walls

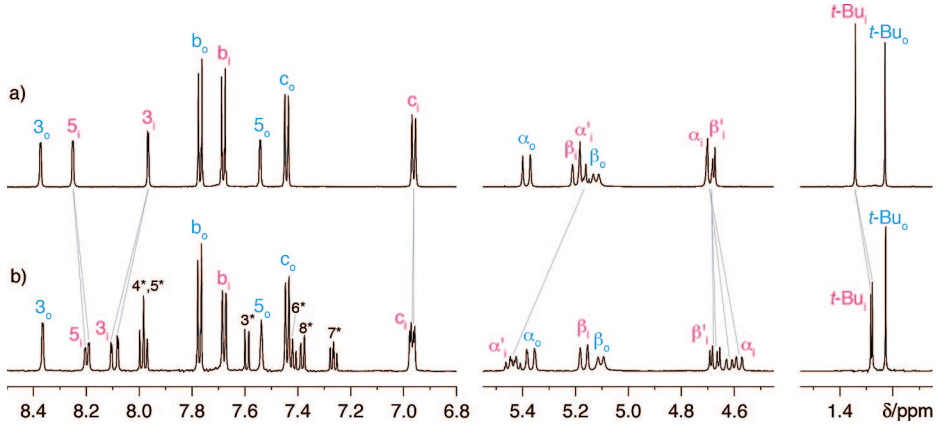

FIGURE 13. Comparison of selected regions of the ^{1}H NMR spectra (600 MHz, acetone-d_6, 298 K) of (a) [**1**•H](CF_3CO_2). (b) [**1**•H][(*R*)-(−)-BNP]. Gray lines show the shifts induced by substitution of the $CF_3CO_2^-$ anion for BNP$^-$. The asterisks label protons of the BNP$^-$ anion.

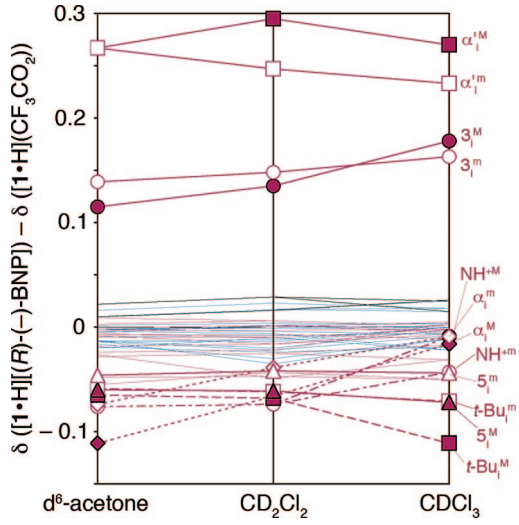

FIGURE 14. Plot of the chemical shift difference ($\Delta\delta$, ppm) between analogous protons of [**1**•H][(*R*)-(−)-BNP] and [**1**•H](CF_3CO_2) in acetone-d_6, CD_2Cl_2, and $CDCl_3$. Curves corresponding to the protons undergoing the largest $\Delta\delta$ are highlighted.

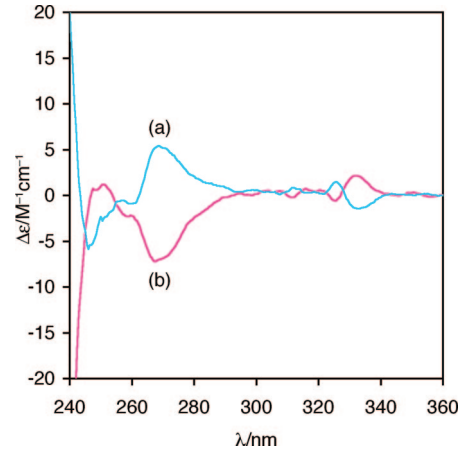

FIGURE 15. Difference spectra of (a) [**1**•H][(*S*)-(+)-BNP] and [Et_3NH][(*S*)-(+)-BNP]; (b) [**1**•H][(*R*)-(−)-BNP] and [Et_3NH][(*R*)-(−)-BNP)] in $CHCl_3$.

of this cavity are placed in the shielding region of the other. Conversely, further evidence for the location of the BNP$^-$ anion arose from ROESY experiments (Figure S39, Supporting Information).[28] Whereas the maps obtained with the standard mixing time of 300 ms did not show any cross-peak between protons of the anion and protons of the cation, increasing the value of this parameter to 600−800 ms allowed to observe NOE contacts between proton 3 of BNP$^-$ on the one hand, and *t*-Bu_i (acetone-d_6) or 3_i ($CDCl_3$) of [**1**•H]$^+$ on the other hand. This explains why proton 3 of BNP$^-$ experiences the strongest deshielding (up to +0.114 ppm in acetone-d_6), due to its positioning in the deshielding field of the endo $N(CH_2Ar)_3$ propellers (Table S12, Supporting Information).

As optically active BNP$^-$ gave the best asymmetric induction in $CDCl_3$, the optical activities of the ion pairs [**1**•H][(*R*)-(−)-BNP] and [**1**•H][(*S*)-(+)-BNP] were measured by circular dichroism in $CHCl_3$. The spectra of [**1**•H][(*R*)-(−)-BNP], [**1**•H][(*S*)-(+)-BNP], and those of the reference compounds [Et_3NH][(*R*)-(−)-BNP] and [Et_3NH][(*S*)-(+)-BNP)] are shown in Figure S40 (Supporting Information). The difference spectra, which should allow us, in principle, to evaluate the induced circular dichroism (ICD) of [**1**•H]$^+$, are reproduced in Figure 15.

The spectra of [**1**•H][(*R*)-(−)-BNP] and [Et_3NH][(*R*)-(−)-BNP] are quasi-superposable above 300 nm where they are dominated by features of the [(*R*)-(−)-BNP]$^-$ anion. The same is true for the spectra of species that contain [(*S*)-(+)-BNP]$^-$ instead. This indicates that at concentrations 10^3 times smaller than those used in the ^{1}H NMR experiments, BNP$^-$ remains associated with [**1**•H]$^+$. It is also interesting to note that these spectra are practically superposable upon dilution by a factor of 10 (concentration range: $5.38 \times 10^{-4} - 5.10 \times 10^{-5}$ mol L^{-1}). The difference spectra are almost mirror-image above 260 nm. Below this value, the baseline slightly deviates toward negative values of $\Delta\varepsilon$. Maxima with mean values of $\Delta\varepsilon$ can be noted at 265 (±5.83), 311 (±0.49), 325 (±0.98), and 331 nm (±1.69 mol^{-1} L cm^{-1}). The latter three weak bands correspond to the BNP$^-$ anion, because [**1**•H]$^+$ does not absorb in the low energy region of the UV spectrum. This means that the conformation and chiroptical properties of BNP$^-$ are changed as the result of its association with [**1**•H]$^+$ and conversely. As a consequence, rather than strictly representing the ICD of BNP$^-$ on [**1**•H]$^+$, the difference spectra of Figure 15 are the chiroptical expression of the mutual interactions between the BNP$^-$ anion and [**1**•H]$^+$. These facts indicate that [**1**•H]$^+$ and BNP$^-$ form a tight ion pair, even in diluted solutions. A maximal $\Delta\varepsilon$ value of ± 24 mol^{-1} L cm^{-1} at λ = 265 nm can be estimated,

(28) (a) Rugutt, J. K.; Billiot, E.; Warner, I. M. *Langmuir* **2000**, *16*, 3022–3029. (b) Macchioni, A. *Eur. J. Inorg. Chem.* **2003**, 195–205.

assuming that the 24% de value measured at 1.66×10^{-2} mol L^{-1} is independent of concentration. This relatively low value of the ICD can be explained by the fact that the orientation of the *exo* $N(CH_2Ar)_3$ propellers is opposite to that of the *endo* ones (Figure 3).

Summary and Conclusion

The sterically crowded $[N_2S_6]$ macropentacycle **1**, a molecule related to diazabicycloalkanes and cryptands, converts slowly into the thermodynamic i^+o form upon reaction with Brønsted acids. The monoprotonated i^+o $[\mathbf{1}\cdot H]^+$ form is C_3 helically chiral in the solid state and in solution, and the structures obtained by single-crystal X-ray diffraction and ^1H NMR can be fully correlated. The proton is encapsulated in the tetrahedral coordination sphere provided by the *endo* bridgehead nitrogen and the three proximal thioether sulfurs, which makes this system a complex of proton rather than a protonated tertiary amine. Contrary to diaza-macrobicycle [4.4.4]-**2**, cryptand [1.1.1]-**3**, and aza-cryptand **4**, macropentacycle **1** does not behave as a "proton sponge" because it can be deprotonated using an excess of bases such as DABCO or sodium methoxide. A significant induction of chirality (up to 24% de in $CDCl_3$) was observed by ion pairing of the $[\mathbf{1}\cdot H]^+$ cation with optically active 1,1′-binaphthyl-2,2′-diyl phosphate ([(*R*)-(−)-BNP]$^-$ or [(*S*)-(+)-BNP]$^-$) anion. Detailed NMR studies allowed us to locate the chiral anion on the *endo* side of $[\mathbf{1}\cdot H]^+$, in the cavity lined by protons α'_i, 3_i and the *t*-Bu_i groups, and to establish that the rate of anion exchange in $[\mathbf{1}\cdot H][(S,R)\text{-}(\pm)\text{-BNP}]$ was higher than the rate of propeller inversion of $[\mathbf{1}\cdot H]^+$. A limiting $\Delta\varepsilon$ value of $\pm$ 24 mol^{-1} L cm^{-1} at $\lambda = 265$ nm for the induced optical activity (ICD) of the enantiomers $[\mathbf{1}\cdot H][(R)\text{-}(-)\text{-BNP}]$ and $[\mathbf{1}\cdot H][(S)\text{-}(+)\text{-BNP}]$ in chloroform was estimated by CD spectroscopy. The relatively low value of de could be explained by the fact that the ion pair does not have the optimal structure for efficient transfer of chiral information. Indeed, it involves species belonging to incommensurate symmetry point groups (respectively C_2 and C_3). Ongoing studies involve D_3 symmetric anions and will be reported in due course.

This work has also shown that $[\mathbf{1}\cdot H]^+$ forms tight ion pairs with various anions ($CF_3SO_3^-$, $CF_3CO_2^-$, Cl^-), including optically active ones (BNP^-), which makes this proton complex behave as an anion receptor. As shown by X-ray crystallography and ^1H NMR spectroscopy, the anions are recognized by the external cavity of $[\mathbf{1}\cdot H]^+$, which is lined by the *endo* *t*-Bu groups, most probably by charged $^+HN-CH\cdots X^-$ hydrogen bond interactions. This suggests that the proton complex $[\mathbf{1}\cdot H]^+$ could be possibly used as anion sensor, for example, by monitoring the complexation induced shifts of relevant protons.

Experimental Section

X-ray Crystallography. Prismatic ($0.25 \times 0.12 \times 0.10$ mm^3), colorless single-crystals of $[\mathbf{1}\cdot H](Cl)\cdot 7C_3D_6O\cdot 2H_2O$ were grown by slow evaporation of acetone-d_6 solutions. A specimen of good crystal quality was selected for the X-ray diffraction experiment at $T = 115(2)$ K. The X-ray source was graphite-monochromatized Mo Kα radiation ($\lambda = 0.71073$ Å) from a sealed tube. Measurements were collected on a Nonius KappaCCD diffractometer,[29] equipped with a nitrogen jet stream low-temperature system (Oxford Cryosystems). Intensity data were recorded as ω- and φ-scans with κ-offsets. Data reduction was done by using the DENZO software.[30] The structure was solved by direct methods using the SIR97 program.[31] Because of the large number of parameters (1789), the refinement of the crystal structure could not be carried out by full-matrix least-squares methods on F^2. Instead, it was undertaken by full-matrix-block least-squares methods on F^2, using BLOC instructions as implemented in the SHELXL97 program.[32] This procedure has allowed us to refine alternatively two sets of roughly a half of the total number of parameters (993 and 798) in a cyclic manner until convergence. Seven C_3D_6O deuterated acetone and two water molecules cocrystallized with $[\mathbf{1}\cdot H](Cl)$. Each water molecule was found disordered over two close positions and was refined by fixing its site occupation factors (sof) at 0.75/0.25. Most hydrogen atoms were found in the Fourier synthesis. They were placed at calculated positions using a riding model, except those observed for one water molecule exhibiting a sof of 0.75, which were refined with restrained distance (Ow−H ∼ 0.98 Å) and angle (H−Ow−H ∼ 107°), as observed in water molecules from neutron diffraction experiments. The other water hydrogen atoms were not found. The $N-H^+$ hydrogen atom was restrained to the mean observed distance for protonated nitrogens from neutron data (∼1.033 Å). The isotropic thermal displacements of all hydrogen atoms were fixed at 1.3 times the U_{iso} value observed for their bonded atom. Crystallographic views were generated using ORTEP III for Windows.[33]

CD Spectroscopy. CD experiments were run with a spectropolarimeter equipped with a xenon lamp, using quartz cuvettes with a 0.1 cm optical path.

Synthesis. The preparation of macropentacycle **1** and its proton adduct $[\mathbf{1}\cdot H](CF_3SO_3)$ has been reported in ref 14b. Analytical data for the latter are reported in the Supporting Information. All protonation reactions were monitored by TLC (SiO_2; CH_2Cl_2/CH_3OH 98:2 for CF_3CO_2H, and 97:3 for BNPH).

$[\mathbf{1}\cdot H](CF_3CO_2)$. Trifluoroacetic acid (0.68 μL, 8.79×10^{-6} mol) was added to a solution of **1** (0.021 g, 8.79×10^{-6} mol) in CH_2Cl_2 (1 mL). After completion of the reaction, the solvent was removed under vacuum and the product used without purification (quantitative yield): ^1H NMR (CD_2Cl_2, 600 MHz, 300 K) δ 9.397 (br q, 1 H; N*H*$^+$), 8.314 (d, $^4J = 2.4$ Hz, 3 H; 3_o), 7.992 (d, $^4J = 1.8$ Hz, 3 H; 5_i), 8.855 (d, $^4J = 2.4$ Hz, 3 H; 3_i), 7.671 (d, $^3J = 8.4$ Hz, 6 H; b_o), 7.633 (d, $^3J = 8.4$ Hz, 6 H; b_i), 7.372 (d, $^3J = 8.4$ Hz, 6 H; c_o), 7.183 (d, $^4J = 1.8$ Hz, 3 H; 5_o), 6.948 (d, $^3J = 8.4$ Hz, 6 H; c_i), 5.295 (d, $^2J = 16.8$ Hz, 3 H; α_o), 5.134 (dd, $^2J = 13.2$ Hz, $^3J = 10.2$ Hz, 3 H; α'_i), 5.120 (d, $^2J = 13.8$ Hz, 3 H; β_o), 5.094 (d, $^2J = 16.8$ Hz, 3 H; β_i), 4.612 (d, $^2J = 16.8$ Hz, 3 H; β'_i), 4.422 (d, $^2J = 12.0$ Hz, 3 H; α_i), 4.070 (d, $^2J = 16.8$ Hz, 3 H; α'_o), 3.724 (d, $^2J = 12.0$ Hz, 3 H; β'_o), 3.629 (ddd, $^2J = 13.8$ Hz, $^3J = 2.4$ Hz, $^3J = 2.4$ Hz, 3 H; ε'_o), 3.513 (ddd, $^2J = 15.6$ Hz, $^3J = 12.0$ Hz, $^3J = 3.6$ Hz, 3 H; γ'_i), 3.094 (ddd, $^2J = 13.8$ Hz, $^3J = 13.8$ Hz, $^3J = 2.4$ Hz, 3 H; ε_o), 3.016 (ddd, $^2J = 14.4$ Hz, $^3J = 10.8$ Hz, $^3J = 3.6$ Hz, 3 H; γ_o), 2.891 (ddd, $^2J = 15.6$ Hz, $^3J = 12.0$ Hz, $^3J = 3.6$ Hz, 3 H; γ_i), 2.679 (ddd, $^2J = 14.4$ Hz, $^3J = 4.2$ Hz, $^3J = 4.2$ Hz, 3 H; γ'_o), 2.438 (s, 9 H; e_o), 2.285 (ddd, $^2J = 13.8$ Hz, $^3J = 3.0$ Hz, $^3J = 3.0$ Hz, 3 H; ε_i), 2.207 (s, 9 H; e_i), 1.666 (ddd, $^2J = 13.8$ Hz, $^3J = 2.4$ Hz, $^3J = 2.4$ Hz, 3 H; ε'_i), 1.296 (s, 27 H; *t*-Bu_i), 1.180 (s, 27 H; *t*-Bu_o), 1.031 (m, 3 H; δ), 0.517 (br q, 3 H; δ′), and Tables S6 and S10, Supporting Information; ^{13}C NMR, Tables S7, S9, and S11, Supporting Information.

$[\mathbf{1}\cdot H][(R)\text{-}(-)\text{-BNPH}]$. A solution of [(*R*)-(−)-BNPH] (0.00325 g, 0.00933 mmol) in methanol (1.2 mL) was added to a solution of macropentacycle **1** (0.0224 g, 0.00933 mmol) in dichloromethane (3.8 mL). Solvents were evaporated after 24 h of stirring, leaving $[\mathbf{1}\cdot H][(R)\text{-}(-)\text{-BNP}]$ quantitatively. Slow evaporation of a solution

(29) Nonius COLLECT, Data Collection Software; Nonius, B. V.: Delft, The Netherlands, 1998.

(30) Otwinowski, Z.; Minor, W. *Methods Enzymol.* **1997**, *276*, 306–326.

(31) Altomare, A.; Burla, M. C.; Camalli, M.; Cascarano, G. L.; Giacovazzo, C.; Guagliardi, A.; Moliterni, A. G. G.; Polidori, G.; Spagna, R. *J. Appl. Crystallogr.* **1999**, *32*, 115–119.

(32) Sheldrick, G. M. *SHELXS-97 Program for the Solution of Crystal Structures*; University of Göttingen: Göttingen, Germany, 1997.

(33) Farrugia, L. J. *J. Appl. Crystallogr.* **1999**, *32*, 837–838.

of the crude material in a 1:2 mixture of dichloromethane/benzene (3 mL) afforded colorless crystals of [**1**·H][(*R*)-(−)-BNP] (0.0243 g, 95% yield): ^{1}H NMR (CD_2Cl_2, 600 MHz, 300 K) δ 9.32 (br q, 1 H; NH^+), 8.306 (d, ^4J = 1.8 Hz, 3 H; 3_o), 8.003 (d, ^4J = 2.4 Hz, 1.26 H; 3_i^m), 7.990 (d, ^4J = 2.4 Hz, 1.74 H; 3_i^M), 7.950 (d, ^4J = 1.8 Hz, 1.26 H; 5_i^m), 7.948 (d, ^3J = 9.0 Hz, 2 H; 4-BNP), 7.931 (d, ^4J = 1.8 Hz, 1.74 H; 5_i^M), 7.916 (d, ^3J = 8.7 Hz, 2 H; 5-BNP), 7.675 (d, ^3J = 8.4 Hz, 6 H; b_o), 7.633 (d, ^3J = 8.4 Hz, 3.48 H; b_i^M), 7.630 (d, ^3J = 8.4 Hz, 2.52 H; b_i^m), 7.613 (d, ^3J = 9 Hz, 2 H; 3-BNP), 7.414 (ddd, 2 H; 6-BNP), 7.412 (d, 2 H; 8-BNP), 7.373 (d, ^3J = 8.4 Hz, 6 H; c_o), 7.244 (ddd, ^3J = 8.4 Hz, ^3J = 6.6 Hz, ^4J = 1.2 Hz, 2 H; 7-BNP), 7.185 (br s, 3 H; 5_o), 6.954 (d, ^3J = 8.4 Hz, 3 H; c_i), 5.429 (dd, ^2J = 13.2 Hz, ^3J = 10.2 Hz, 1.74 H; $\alpha'_i{}^M$), 5.381 (dd, ^2J = 13.2 Hz, ^3J = 10.2 Hz, 1.26 H; $\alpha'_i{}^m$), 5.281 (d, ^2J = 16.8 Hz, 1.74 H; $\alpha_o{}^M$), 5.273 (d, ^2J = 16.8 Hz; $\alpha_o{}^m$), 5.096 (br d, ^2J = 15.6 Hz, 3 H; β_o), 5.069 (br d, ^2J = 16.8 Hz, 3 H; β_i), 4.596 (d, ^2J = 16.8 Hz, 3 H; β'_i), 4.383 (br d, ^2J = 12.6 Hz, 1.26 H; $\alpha_i{}^m$), 4.356 (br d, ^2J = 12.6 Hz, 1.74 H; $\alpha_i{}^M$), 4.058 (d, ^2J = 16.8 Hz, 1.74 H; $\alpha'_o{}^M$), 4.050 (d, ^2J = 16.8 Hz, 1.26 H; $\alpha'_o{}^m$), 3.741 (br d, ^2J = 12.0 Hz, 3 H; β'_o), 3.608 (ddd, ^2J = 14.4 Hz, ^3J = 14.4 Hz, ^3J = 2.4 Hz, 1.74 H; $\varepsilon'_o{}^M$), 3.585 (ddd, ^2J = 14.4 Hz, ^3J = 14.4 Hz, ^3J = 2.4 Hz, 1.26 H; $\varepsilon'_o{}^m$), 3.506 (ddd, ^2J = 15.6 Hz, ^3J = 12.0 Hz, ^3J = 4.2 Hz, 3 H; γ'_i), 3.088 (ddd, ^2J = 13.8 Hz, ^3J = 13.8 Hz, ^3J = 3.2 Hz, 1.26 H; $\varepsilon_o{}^m$), 3.084 (ddd, ^2J = 14.2 Hz, ^3J = 14.2 Hz, ^3J = 2.6 Hz, 1.74 H; $\varepsilon_o{}^M$), 3.012 (ddd, ^2J = 14.2 Hz, ^3J = 10.8 Hz, ^3J = 3.6 Hz, 3 H; γ_o), 2.881 (br ddd, ^3J = 13.2 Hz, 3 H; γ_i), 2.792 (br ddd, 1.74 H; $\gamma'_o{}^M$), 2.786 (br ddd, ^2J = 14.4 Hz, 1.26 H; $\gamma'_o{}^m$), 2.438 (s, 9 H; e_o), 2.242 (ddd, ^2J = 13.8 Hz, 1.74 H; $\varepsilon_i{}^M$), 2.238 (ddd, ^2J = 12.6 Hz, 1.26 H; $\varepsilon_i{}^m$), 2.209 (s, 9 H; e_i), 1.644 (ddd, ^2J = 13.8 Hz, ^3J = 13.8 Hz, ^3J = 2.4 Hz, 1.74 H; $\varepsilon'_i{}^M$), 1.617 (ddd, ^2J = 13.8 Hz, ^3J = 13.8 Hz, ^3J = 2.4 Hz, 1.26 H; $\varepsilon'_i{}^m$), 1.234 (s, 11.34 H; t-Bu_i^m), 1.228 (s, 15.66 H; t-Bu_i^M), 1.180 (s, 11.34 H; t-Bu_o^m), 1.179 (s, 15.66 H; t-Bu_o^M), 1.047 (m, 3 H; δ), 0.546 (br q, 3 H; δ'), and Tables S6, S8, and S10, Supporting Information; ^{13}C NMR (CD_2Cl_2, 151 MHz, 298 K) δ 154.9 (4_i), 153.1 (4_o), 150.9 (d; 2-BNP), 144.5 (d_o), 144.0 (2_o), 143.6 (d_i), 142.19 (6_i^m), 142.14 (6_i^M), 140.8 (6_o), 139.5 (a_i), 134.63 (2_i^M), 134.60 (2_i^m), 134.2 (a_o), 133.1 (9-BNP), 132.96 (3_i^m), 132.88 (3_i^M), 132.54 (1_i^m), 132.48 (1_i^M), 131.56 (d, 1_o), 131.3 (10-BNP), 130.3 (c_o), 130.2 (4-BNP), 130.0 (c_i), 129.46 (5_i^m), 129.38 (5_i^M), 128.6 (5-BNP), 128.1 (5_o), 128.0 (b_o), 127.4 (b_i), 127.4 (8-BNP), 126.1 (7-BNP), 124.7 (6-BNP), 124.6 (3_o), 123.0 (1-BNP), 122.9 (3-BNP), 57.67 (α_i^m), 57.61 (α_i^M), 55.8 (α_o), 55.6 (β_o), 48.9 (β_i), 46.9 (d; γ_i), 46.7 (γ_o), 42.8 (ε_i^M), 42.7 (ε_i^m), 41.21 (ε_o^M), 41.17 (ε_o^m), 35.40 (($C(CH_3)_3)_i^m$), 35.38 (($C(CH_3)_3)_i^M$), 35.0 (($C(CH_3)_3)_o$), 31.2 (($C(CH_3)_3)_o$), 31.1 (($C(CH_3)_3)_i$), 26.0 (δ), 21.65 (e_o), 21.50 (e_i), and Tables S7 and S11, Supporting Information. Anal. Calcd for $C_{149}H_{175}N_8O_{16}PS_{12}\cdot CH_2Cl_2$ (2834.77): C, 63.56; H, 6.29; N, 3.95; S, 13.57. Found: C, 63.49; H, 6.26; N, 3.73; S, 13.57.

[Et$_3$NH][(*R*)-(−)-BNP]. Triethylamine (0.140 mL, 1 mmol) was added to a suspension of [(*R*)-(−)-BNPH] (0.349 g, 1 mmol) in methanol (10 mL). After 30 min of stirring, the solution was concentrated on a rotary evaporator. The dry residue was dissolved in boiling ethanol (10 mL). After cooling to room temperature, 0.238 g of crystals of [Et_3NH][(*R*)-(−)-BNP] were obtained: yield 53%; ^{1}H NMR (CD_2Cl_2, 600 MHz, 298 K) δ 11.88 (br s, 1 H; NH^+), 7.97 (d, ^3J = 9.0 Hz, 2 H; 4-H), 7.93 (br d, ^3J = 8.4 Hz, 2 H; 5-H), 7.54 (dd, $^3J_{H,H}$ = 9.0 Hz, $^4J_{H,P}$ =1.2 Hz, 2 H; 3-H), 7.42 (br ddd, ^3J = 8.4 Hz, ^3J = 7.2 Hz, ^4J = 1.2 Hz, 2 H; 6-H), 7.36 (br d, ^3J = 8.4 Hz, 2 H; 8-H), 7.26 (ddd, ^3J = 8.4 Hz, ^3J = 7.2 Hz, ^4J = 1.2 Hz, 2 H; 7-H), 2.83 (m, 6 H; CH_2), 1.14 (t, ^3J = 7.2 Hz; CH_3), and Table S12, Supporting Information; ^{13}C NMR (CD_2Cl_2, 151 MHz, 298 K) δ 150.0 (d, $^2J_{C,P}$ = 9 Hz; 2), 133.0 (s; 9), 131.4 (s; 10), 130.4 (s; 4), 128.6 (s; 5), 127.2 (s; 8), 126.4 (s; 7), 125.0 (s; 6), 122.7 (d, $^3J_{C,P}$ = 3 Hz; 1), 122.4 (d, $^3J_{C,P}$ = 3 Hz; 3), 46.0 (s; CH_2), 8.6 (s, CH_3), and Table S12, Supporting Information. Anal. Cacld for $C_{26}H_{28}NO_4P$ (449.49): C, 69.48; H, 6.28; N, 3.12. Found: C, 69.76; H, 6.48; N, 3.12.

Kinetics of Protonation of 1 with CF_3SO_3H and CF_3CO_2H. CF_3SO_3H (1 μL, 0.0112 mmol) was added to a solution of macropentacycle **1** (0.027 g, 0.0112 mmol) in dry $CDCl_3$ or CD_2Cl_2 (0.5 mL). ^{1}H NMR spectra were recorded at regular intervals at 300 K. Under the same conditions, protonation with CF_3CO_2H is immediate.

Supporting Information Available: Analytical data for [**1**·H](CF_3SO_3). Preparation and characterization of [**1**·H][(*S*)-(+)-BNP], [**1**·H][(*S*,*R*)-(±)-BNP], and [Et_3NH][(*S*)-(+)-BNP]. Crystallographic data for [**1**·H](Cl) and additional ORTEP views for [**1**·H](CF_3SO_3). Determination of dihedral angles from the vicinal coupling constants. Copies of the ^{13}C, ^{1}H/^{1}H COSY and ROESY, ^{13}C/^{1}H HSQC and HMBC NMR spectra for [**1**·H](CF_3CO_2) in CD_2Cl_2, and pictorial representations of the corresponding correlations. VT ^{1}H NMR spectra of [**1**·H]-(CF_3SO_3) in $C_2D_2Cl_4$ and CD_2Cl_2. Time evolution of the ^{1}H NMR spectrum of **1** + CF_3SO_3H (1 equiv) in $CDCl_3$ and CD_2Cl_2. Copies of the ^{1}H and ^{13}C, ^{1}H/^{1}H COSY, ^{13}C/^{1}H HSQC, and HMBC NMR spectra of [Et_3NH][(*R*)-(−)-BNP] in CD_2Cl_2. Copies of the ^{1}H and ^{13}C NMR spectra of [**1**·H][(*R*)-(−)-BNP] in CD_2Cl_2. Time evolution of the ^{1}H NMR spectrum of **1** + [(*R*)-(−)-BNPH]. VT ^{1}H NMR spectra of [**1**·H][(*R*)-(−)-BNP] in $CDCl_3$. Detail of the ^{1}H/^{1}H ROESY NMR spectrum of [**1**·H][(*R*)-(−)-BNP] in acetone-d_6 and $CDCl_3$. CD spectra of [Et_3NH][(*R*)-(−)-BNP], [Et_3NH][(*S*)-(+)-BNP], [**1**·H][(*R*)-(−)-BNP], and [**1**·H][(*S*)-(+)-BNP] in $CHCl_3$. Tables of the chemical shifts (proton and carbon) of [**1**·H][(*R*)-(−)-BNP] and [**1**·H](CF_3CO_2) in $CDCl_3$, CD_2Cl_2, and acetone-d_6. Table of the proton and carbon chemical shifts of [(*R*)-(−)-BNP]$^-$ in its salts with [**1**·H]$^+$ and Et_3NH^+. This material is available free of charge via the Internet at http://pubs.acs.org.

JO801438D